

EXPERIMENTAL STUDY ON THE BEHAVIOUR OF L-SHAPED COLUMNS FABRICATED USING CONCRETE-FILLED STEEL TUBES UNDER ECCENTRIC LOADS

Qing-Qing Xiong¹, Wang Zhang^{1,*}, Zhi-Hua Chen², Ting Zhou³ and Jia-Hui Qian¹

¹ School of Civil Engineering, Shijiazhuang Tiedao University, Shijiazhuang, China

² Department of Civil Engineering, Tianjin University, Tianjin, China

³ Department of Architecture, Tianjin University, Tianjin, China

* (Corresponding author: E-mail: zhangwang@stdu.edu.cn)

ABSTRACT

In this study, the eccentric compression properties of L-shaped columns fabricated using concrete-filled steel tubes connected by double vertical steel plates (LCFST-D columns) were experimentally studied. The eccentricity was used as a parameter to analyse the deformation development, failure mode and ultimate carrying capacity of these columns. The test result indicated that the LCFST-D columns had a good ductility and bearing capacity. Compared with LCFST columns under identical eccentricity, the LCFST-D columns had a higher bearing capacity, over 20%, and significantly higher ductility. The double vertical steel plates filled with concrete efficiently improved the collaboration among the monocolumns, strengthened their integrity and fully utilized the material properties. The test study used a finite element model to analyse the entire deformation process of LCFST-D columns and the interaction among monocolumns to determine the effects of the eccentricity, vertical steel plate thickness, and steel pipe thickness on the performance of these columns under eccentric compression. The test result showed that overall bending and buckling were the failure modes of the LCFST-D columns, during which the three monocolumns bulged first. The eccentricity was a key factor that affected the eccentric load bearing capacity of these columns. Increasing the eccentricity notably decreased the bearing capacity of the columns. Increasing the steel pipe thickness delayed the local buckling of a monocolumn, which increased its bearing capacity. Based on this analysis, a formula to predict the eccentric compression capacity of LCFST-D columns was proposed. The error between calculation results and test data was less than 10%, and the accuracy was verified by the test results.

ARTICLE HISTORY

Received: 18 January 2021
Revised: 29 July 2021
Accepted: 10 August 2021

KEYWORDS

LCFST-D columns;
Eccentric compression experiment;
Finite element analysis;
Compression and bending
behaviour;
Bearing capacity

Copyright © 2022 by The Hong Kong Institute of Steel Construction. All rights reserved.

1. Introduction

A concrete-filled steel tube (CFST) column utilizes the advantages of both concrete and steel tubes, which have a high bearing capacity and ductility [1–9]. Scholars have extensively studied square, rectangular, and circular CFST columns [10–13]. With the development of the application of CFST columns, to enhance the seismic properties and carrying capacity of CFST columns, many academics have introduced special-shaped CFST columns with structural forms [14]. Special-shaped CFST columns have a favourable performance because they combine the advantages of CFST columns and special-shaped columns. The capability of a CFST columns to be mosaicked into walls is the main advantage of this type of column, which enables one to place columns without disturbing the available space of buildings and to reduce the amount of material used. Therefore, this new type of structure has received widespread attention [15–16].

There are three types of special-shaped CFST columns: Special-shaped CFST columns (Fig. 1(a)), multi-cell special-shaped CFST columns [17], and special-shaped columns fabricated using CFSTs [18–19].

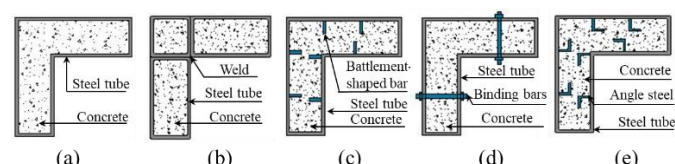


Fig. 1 Different structural forms of L-shaped CFST columns

Special-shaped CFST columns consist of special-shaped steel tubes, e.g., T-shaped, L-shaped, or cross-shaped steel tubes, which are filled with concrete. The major disadvantage of this type of column is the negligible effect of contraction provided by the wall of the steel pipe on the concrete core. After torsion and lateral deformation, large cracks easily form between the concrete and steel pipe on the long side of a special-shaped column, causing a rapid decrease in ductility and bearing capacity. Therefore, many scholars have optimized and improved special-shaped CFST columns [20].

Tu et al. [20] introduced a multi-cell, composite, L-shaped CFST (MS-CFST) column (Fig. 1 (b)). This column is formed by welding three steel pipes together. This column design improves the constraint around the concrete core, but the quality of the vertical welded seam among the steel pipes cannot be

guaranteed.

Yang and Wang et al. [22]–[25] employed a steel rib in an L-shaped CFST column (Fig. 1 (c)). This structure can postpone the partial buckling of the steel pipe, but it cannot effectively improve the constraint surrounding the core concrete. In Zuo et al. [26] and Cai et al. [27], the mechanical performances of L-shaped CFST columns were improved by installing binding bars (Fig. 1 (d)). This method can effectively improve the constraint of the concrete core area and increase the ductility of concrete and bearing capacity. However, there are many holes in this column type, which results in weak areas and easily produces stress concentrations. Lin et al. [28] adopted an approach that included welding angle steel strips longitudinally on the inner surfaces of special-shaped steel tubes, as shown in Fig. 1 (e).

Chen et al. [29–30] introduced a new type of special-shaped CFST column that has a good cooperative working performance and seismic performance. The column was composed of monocolumns connected by steel plates or welded lacing bars. The connection pattern has since been developed from welded lacing bars to vertical steel plates [31–33] (Fig. 2).

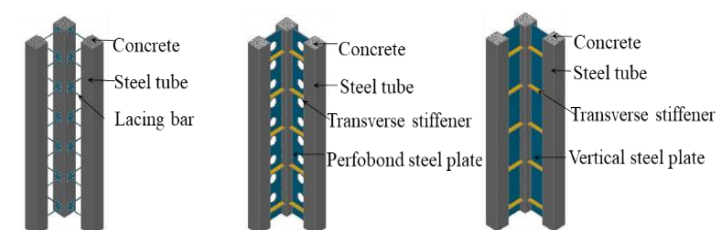


Fig. 2 LCFST column structure

Because columns of concrete-filled steel tubes connected by a vertical steel plate (LCFST columns) have poor monocolumn collaborative performance and their bearing capacity cannot satisfy the demands of high-rise structures, this thesis presents a new type of L-shaped column manufactured using CFSTs connected by double vertical steel plates (LCFST-D columns) (Fig. 3). This mode of connection improves the cooperative performance, adjusts to the characteristics of the materials and improves the bearing capacity. This type of column has good seismic performance. This new structural system has been used in many practical projects (Fig. 4).

In this study, an eccentric compression experiment was performed on

LCFST-D columns. We analysed the mechanical performance and behaviours of LCFST-D columns under eccentric compression by using three-dimensional nonlinear finite element models. This study discussed the effects of the thickness of the steel pipe and steel plate on its eccentric bearing capacity. A calculation method of the slenderness ratio for LCFST-D columns was introduced. The overall stability of the LCFST-D column type was discussed.

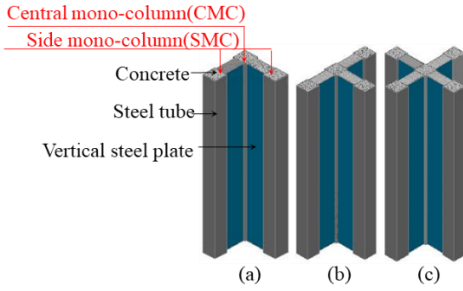


Fig. 3 LCFST-D column structure

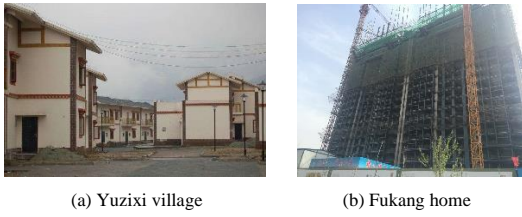


Fig. 4 Practical applications of LCFST-D columns

2. Experimental analyses

2.1. Specimen design and mechanical properties of the materials

In the eccentric compression experiment, the effect of the eccentricity and connection patterns were studied. The LCFST-D columns in this study were labelled D-0, D-40 and D-80, and Fig. 5 (a) shows the details of these test specimens. The LCFST columns in this study were labelled E-0 [33], E-40 [33] and E-80 [33], and Fig. 5 (b) shows the details of these specimens. Table 1 presents the sectional and geometric sizes of the specimens. The height of each specimen was 2000 mm. The steel pipe cross-section sizes were 100 mm × 100 mm × 5.75 mm in the columns. To prevent the partial buckling of both ends of the column during loading, cover plates were welded at both ends of the column. The material strength of a specimen is shown in Table 2.

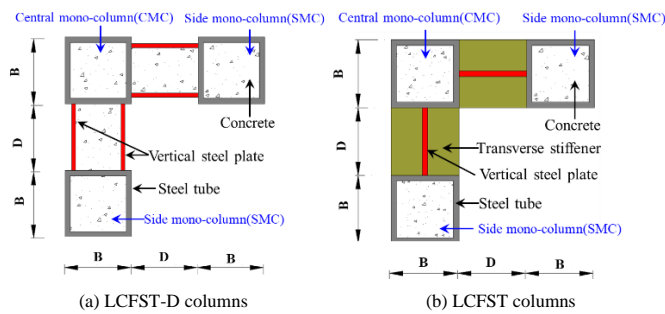


Fig. 5 Details of the test specimens

Table 1
Details of the test specimens

Specimen	L (mm)	Steel tube size (mm)	Vertical steel plate		Eccentricity (mm)
			Width D (mm)	Thickness t_2 (mm)	
D-0	2000	100 × 100 × 5.75	100	5.75	0
D-40	2000	100 × 100 × 5.75	100	5.75	40
D-80	2000	100 × 100 × 5.75	100	5.75	80
E-0 [33]	2000	100 × 100 × 5.75	100	5.75	0
E-40 [33]	2000	100 × 100 × 5.75	100	5.75	40
E-80 [33]	2000	100 × 100 × 5.75	100	5.75	80

Table 2

Mechanical properties of the concrete and steel

Material	Size and thickness (mm)	f_y (MPa)	f_u (MPa)	E_s (MPa)	ε_y ($\mu\epsilon$)
Steel tube	□100 × 5.75	381	476	2.01×10^5	2314
Concrete		$f_c^{1341} = 33.4 \text{ N/mm}^2$			
Vertical steel plate	5.75	368	458	1.75×10^5	1578

2.2. Test setup and loading procedure

This test used a 1000-kN universal testing machine for loading and applied an eccentric load by welding rigid pads at the loading points at both ends of the specimen (Fig. 6). The loading point of a specimen was at the symmetry axis of the specimen, and the eccentricity was tested at 0 mm, 40 mm and 80 mm (Fig. 7).

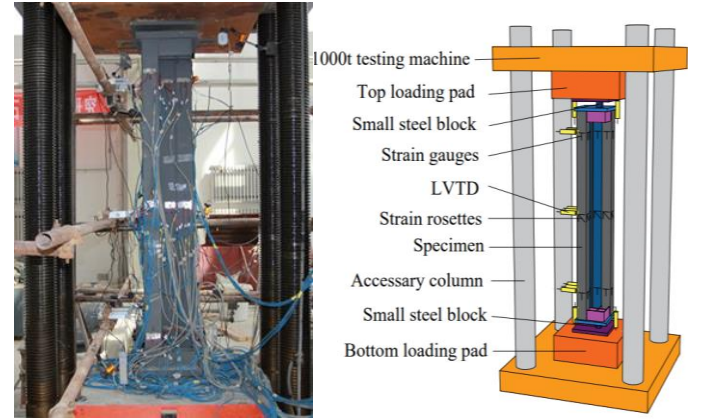


Fig. 6 Test setup and instrumentation layout

The displacement, load and strain were measured by a DH-3816 static strain test system. We measured the longitudinal and lateral displacements by using 19 linear variable displacement transducers (LVDTs). Strain gauges were set on the top, centre and bottom positions of these columns to measure the strain.

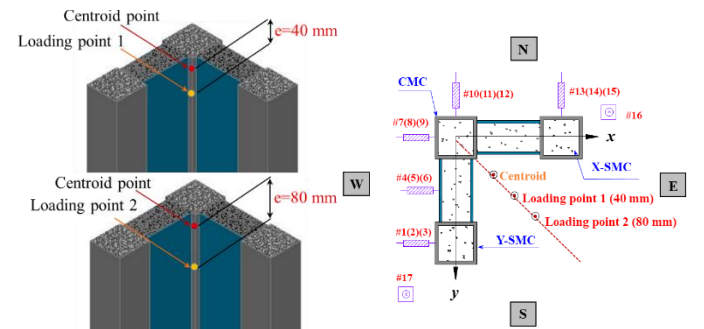


Fig. 7 Arrangement of the loading point and LVDTs

Preloading was conducted before the formal test. The loading method is hierarchical loading. The loads of every phase were approximately 1/10 of the forecasted eccentrically loaded capacity and were applied for 3 min at each grade. The loading stopped when it reached 85% of the peak load.

3. Test results and analysis

3.1. Damage and failure mode

To conveniently describe the test results, the characteristics of the specimens are re illustrated in Fig. 8.

With the continuous increase in lateral deflection, the LCFST-D columns developed obvious bending deformation and finally lost stability. All the specimens showed partial buckling of the monocoolumns after the peak load. D-0 first developed partial buckling, followed by D-40. The welded junction between X-VSP-N/Y-VSP-W and the central monocoolumn (CMC) was pulled,

and cracks appeared 300 mm from the top of D-40, which resulted in stress concentrations at the weld crack. The overall deformation of D-40 did not continuously intensify, but local buckling at the weld crack continuously developed. Finally, D-80 developed local buckling. The failure mode of D-80 was dominated by overall bending deformation with maximum deflection at the middle and local buckling at the column bottom and top (Fig. 9). Specimens with

smaller eccentricities exhibited less overall bending, while the steel pipe and vertical steel plates developed considerable and concentrated local buckling. Conversely, overall bending was the main failure mode of the specimens with larger eccentricities, accompanied by slight local buckling at the ends of the monocolumns. Both D-40 and D-80 exhibited bending and buckling around the weak X'-X' axis.

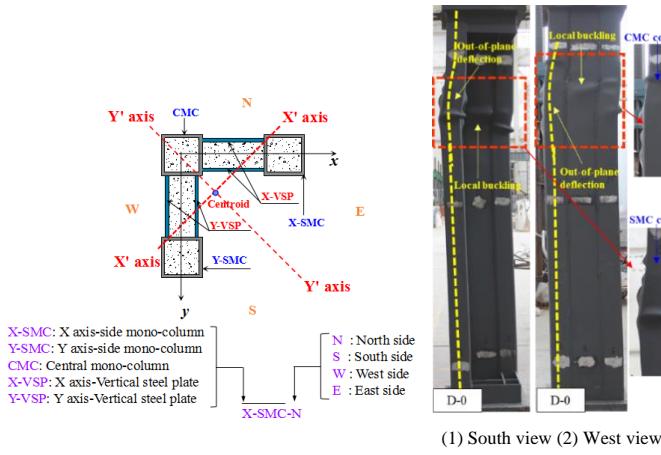


Fig. 8 Features of the specimens

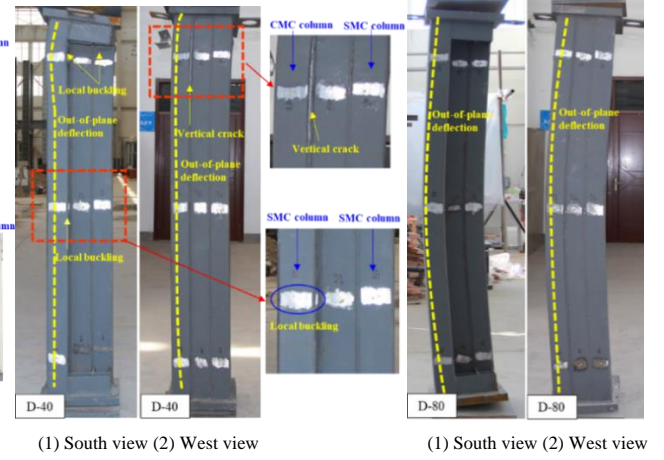


Fig. 9 Failure modes of the tested specimens

3.2. Load-longitudinal displacement response

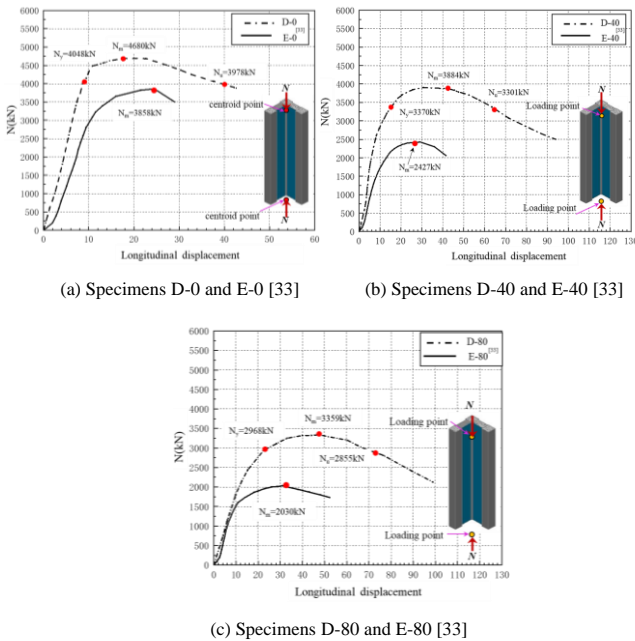


Fig. 10 Load-longitudinal displacement curves of the specimens

The load-lateral deflection curves of these specimens with several eccentricities are shown in Fig. 10. The carrying capacity was sensitive to the eccentricity. When the eccentricity increased, the reduction in the carrying capacity decreased. When the eccentricity increased from 0 to 40 mm (i.e., D-40), the bearing capacity was approximately 17% lower than that of D-0. The bearing capacity of D-40 decreased by approximately 13.5% when the eccentricity further increased to 80 mm (i.e., D-80). Additionally, the ultimate carrying capacity of these specimens, slope of the elastic section of the load-displacement curves, and rigidity decreased, whereas the yield displacement increased, and the descent section became gentler.

The load-displacement curves of the LCFST columns [33] under different eccentricities (0 mm, 40 mm, and 80 mm) are shown in Fig. 9 (d). With identical material properties and section sizes of the monocolumns, the LCFST-D columns exhibited significantly higher carrying capacity than the LCFST columns. With identical eccentricity, the carrying capacities of D-0, D-40, and D-80 were 21.3%, 60%, and 65.5% higher than those of the corresponding LCFST columns (E-0 [33], E-40 [33], and E-80 [33]), respectively.

Table 3

Summary of the test results

Specimen No.	Yield point		Peak point		Ultimate point		SI
	d_y (mm)	N_y (kN)	d_m (mm)	N_m (kN)	d_u (mm)	N_u (kN)	
D-0	9.06	4048	17.6	4680	40.05	3978	1.000
D-40	15.25	3370	42.5	3884	64.7	3301	0.830
D-80	25.4	2968	47.5	3359	73	2855	0.718

Note: d_y is the yielding displacement, N_y is the yielding load, N_m is the peak load, d_m is the maximum displacement, d_u is the ultimate displacement, and N_u is the ultimate load.

3.3. Load-lateral deflection relationship

With increasing eccentricity, the rigidity and peak load decreased, whereas the platform segment of the load-lateral deflection curves increased, which indicates that there was one segment after the peak load in which the specimen loads did not increase but the lateral deflection quickly increased. Moreover, the lateral deflection at the peak load significantly increased. Specimens with smaller eccentricities had longer elastic stages. A larger eccentricity corresponded to a greater growth rate of the lateral deflection (Fig. 11).

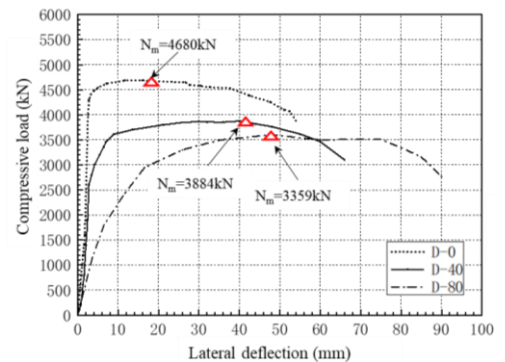


Fig. 11 Load-lateral deflection curves of the middle sections of the specimens

3.4. Load-deflection curves

The load-deflection curves of these columns with several heights and loads are shown in Fig. 12. The X axis-side monocolumn (X-SMC) and Y axis-side monocolumn (Y-SMC) had basically identical load-deflection curves, and the deformation of the LCFST-D column was symmetric. The three monocolumns had similar load-deflection curves, which indicates that the three monocolumns

can coordinate well. The bending deflection in the middle of the CMC was relatively large, whereas the deflection in the middle of the vertical steel plate was relatively small.

Under small loads, the deflection deformation in the middle of the specimens was relatively slight. The deflection growth was basically in direct proportion to the load growth. When the load increased to 70–80% of the peak load, the deflection in the middle of the specimens began to dramatically increase due to the second-order effect. When the deflection at the middle of the specimens reached a critical value, the growth rate of the second-order moment began to exceed the growth rate of the sectional resistance moment, the increase in bearing capacity decelerated, and the deflection in the middle of the specimens sharply increased. The growth rate of the lateral deflection in the middle of the specimens was positively correlated with the eccentricity. The welded joint between the CMC, which is 300 mm from the top of D-40, and the vertical steel plate was pulled and cracked, which caused stress concentrations. Therefore, the local lateral deflection was relatively large. The load-deflection curve of D-80 was symmetric.

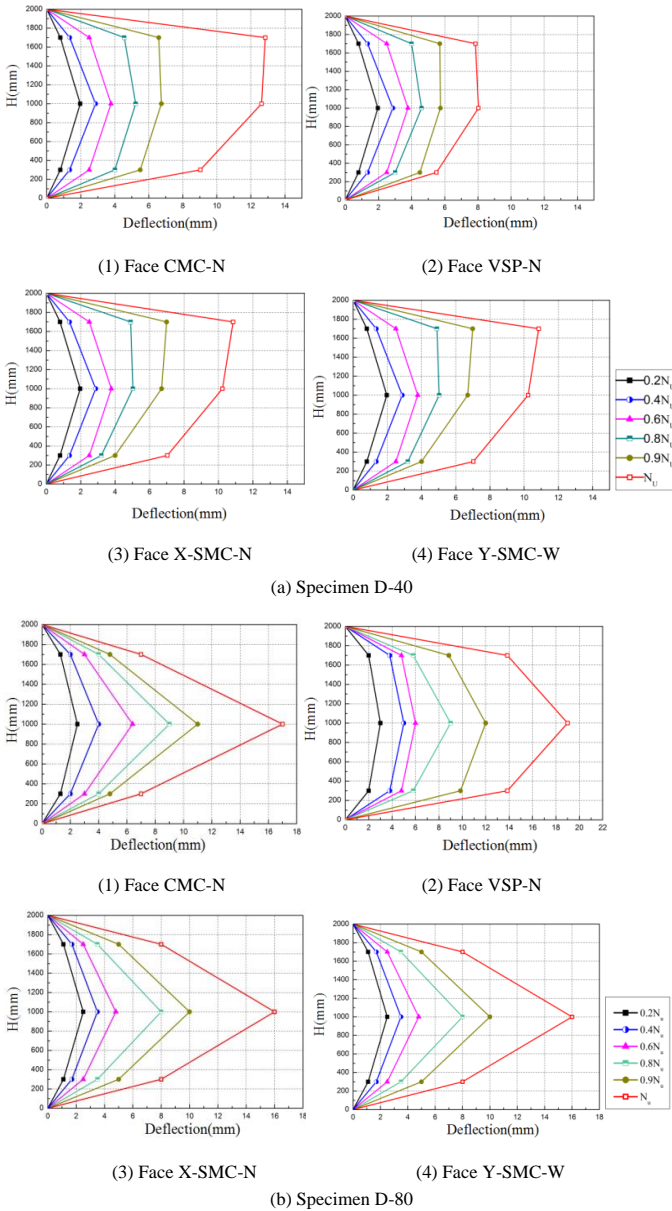


Fig. 12 Load-deflection curves

3.5. Discussion of SI

The carrying capacity of the LCFST-D columns was evaluated based on the strength index (*SI*) as follows [9]:

$$SI = \frac{N_{uc}}{A_s f_y + A_{ps} f_{ps} + A_{pc} f_{pc} + A_c f_c} \quad (1)$$

where A_s is the section area of the steel pipe; f_y is the yield strength of the steel pipe; A_c is the section area of the concrete in the steel pipe; f_c is the compressive strength of the concrete in the steel pipe; A_{ps} is the section area of the vertical steel board; f_{ps} is the yield strength of the vertical steel board; and A_{pc} and f_{pc} are the section area and comprehensive strength of the concrete in the vertical steel board.

The SI decreased with increased eccentricity, and the reduction rate gradually declined. The SI decreased by 17% when the eccentricity was 40 mm, and the SI further decreased by 13.5% when the eccentricity increased to 80 mm. Given the same eccentricity, the LCFST-D columns had notably higher SI than the LCFST columns. The reason is that compared to the steel linking plates, the concrete in the double vertical steel plates effectively enhanced the monocolumn coordination and internal force transmission, prevented the primitive buckling of these vertical steel plates and better utilized the material properties. The SI of D-40 was 30.9% greater than that of E-40, and the SI of D-80 was 35.5% greater than that of E-80 (Fig. 13).

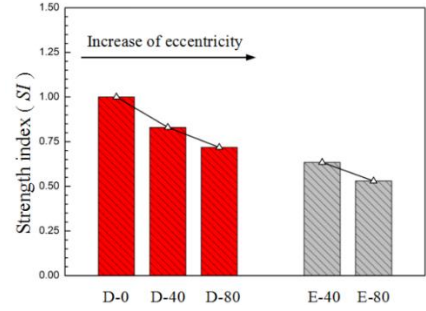
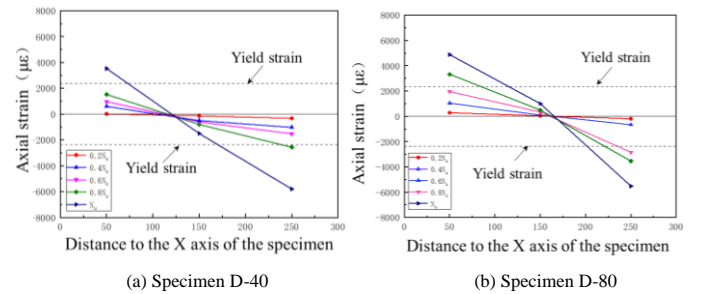


Fig. 13 SI curves of the specimens

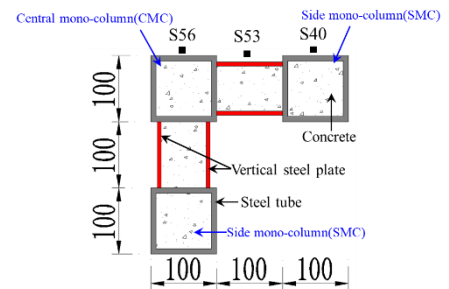
3.6. Vertical strain distributions in the middle cross-section

Fig. 14 shows the distribution of vertical strain under different loading conditions of the evaluated columns. The longitudinal strain in the section increased with increasing load. The CMC bore tension, and the steel plate of the SMC first yielded under pressure. Since the connecting plate was near the neutral axis, the strain was small. Before the load reached 0.6 N_u , the mid-span section strain of the entire specimen was linearly distributed along the section height, and the longitudinal strain basically conformed to the assumption of a flat section. When the load exceeded 0.6 N_u , the strain distribution in the mid-span section along the section height deviated from the assumption of a flat section due to the slight bulge of the steel plate before reaching the peak load. The comparative analysis found that with increasing eccentricity, the growth rate of the longitudinal strain in the CMC and SMC increased.



(a) Specimen D-40

(b) Specimen D-80



(c) Location of strain gauges

Fig. 14 Strain distribution curves of the mid-span cross-section at different stages of specimens

4. Finite element analysis

4.1. Finite element model

To further study the performance of these LCFST-D columns, we established a model using the finite element software ANSYS. In this model, we used SOLID95 elements to establish the steel pipes, vertical connection plates, and cover plates at both ends, whereas SOLID65 elements were used for the concrete in the monocolumns. Fig. 15 shows the meshing of the model.

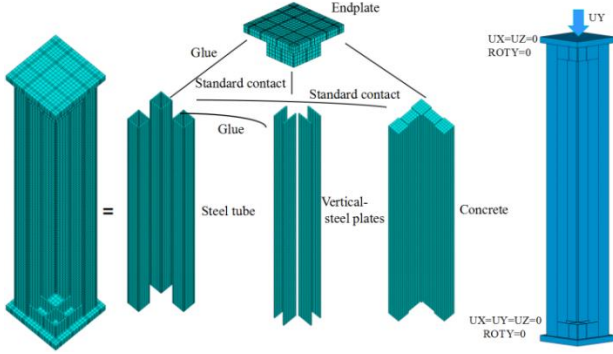


Fig. 15 Assembly and boundary conditions of the analytical model

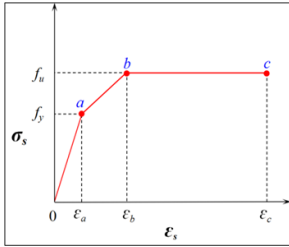


Fig. 16 Stress-strain curve of the concrete

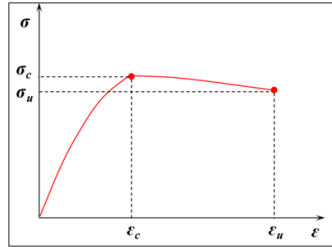


Fig. 17 Stress-strain curve of the steel

In this study, the constitutive curve of the steel tube was obtained by the KINH model [36–38] (Fig. 16). The concrete Poisson's ratio was assumed to be 0.2, while $\epsilon_c = 1.8\sigma_{c0}/E_c$ and $\epsilon_u = 0.0038$, where E_c and σ_{c0} are the elastic modulus and axial compressive strength of the concrete, respectively. The Hognestad constitutive law was adopted for the concrete (Fig. 17).

The boundary conditions of the specimen in the model were consistent with that in the test. The displacement of the column bottom in the X, Y, and Z directions was constrained; the rotation around the Y axis was also restrained. The displacement at the column top was restrained in the X and Z directions. To form a rigid surface, we created a coupling point at the loading point on the column top. Initial defects were considered in the model. The contact element was used to simulate the contact between the steel plate and concrete, and the friction coefficient was 0.4.

4.2. Failure mode and deformation analysis

The finite element analysis found an identical failure mode to that in the experiments, as shown in Fig. 18. Thus, the actual failure can be simulated by finite element analysis (i.e., the accuracy and correctness of the finite element model have been confirmed); hence, the model could be used for the finite element analysis of LCFST-D columns.

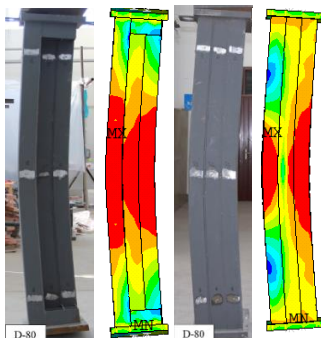


Fig. 18 Final failure mode of a typical specimen

Fig. 19 shows the von Mises stress contours of classical specimens (D-40, D-80) under the yield and peak loads. The LCFST-D column experienced an elastic-plastic stage, an elastic stage, and partial buckling failure. During eccentric loading, the LCFST-D columns exhibited essentially identical stress growth laws. The three monocolumns were first stressed, and the stress on the vertical steel plate gradually increased with continuous loading. The three monocolumns yielded first, and the internal concrete of the SMC reached the maximum stress at the yield load. The middle section of the columns reached the maximum stress, and the entire section yielded at the peak load. Thus, the material properties were fully utilized, which is consistent with the failure mode in the experiment. Therefore, the finite element model is valid.

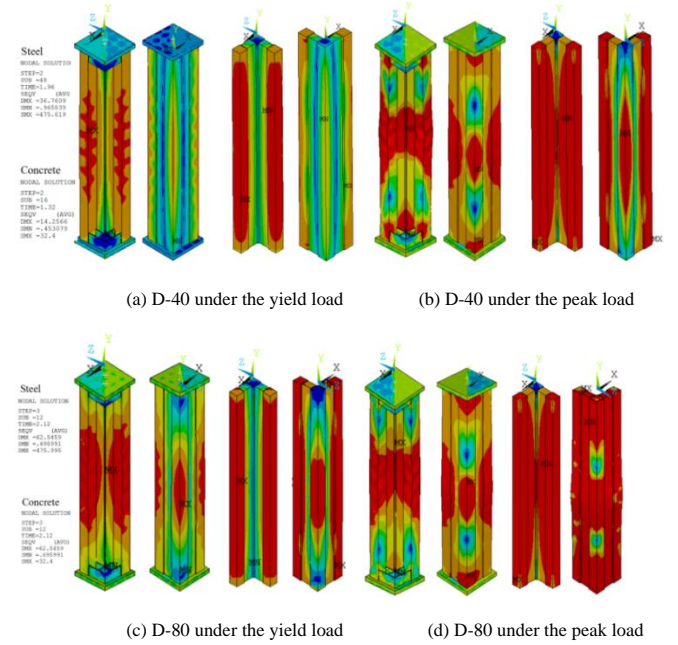


Fig. 19 Contours of von Mises stress for the specimens under the yield and peak loads

4.3. Comparison of the bearing capacity

Fig. 20 shows the curves of the load displacement in the experiment and finite element model. This model could produce the experimentally observed load-displacement curves with good accuracy. The errors between the experimental results and imitation results were less than 5%. The peak load error was 1.4–4.6%. The total error of N_m was 3.1%. The initial rigidity obtained from the finite element analysis was slightly higher than the experimental results because of the initial flaw of the specimen and unevenness of the material.

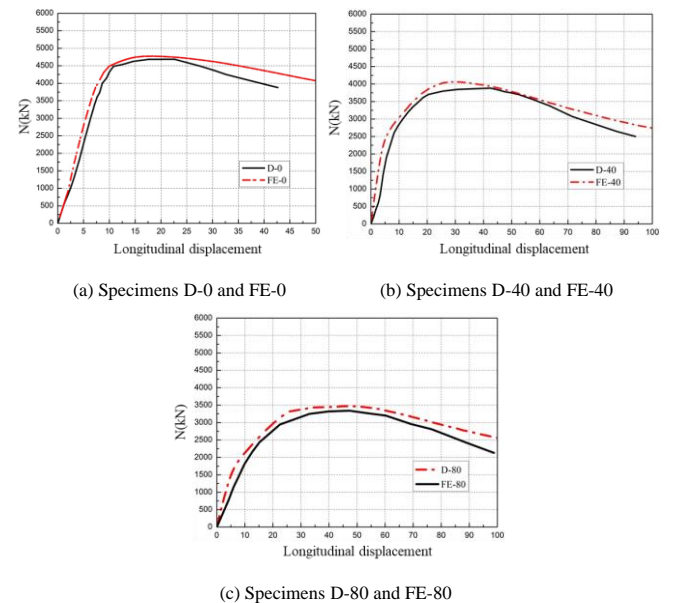


Fig. 20 Comparison of the load-longitudinal displacement curves of the specimen

4.4. Parametric studies

A parametric analysis of the thicknesses of the vertical steel plate and steel pipe was conducted using the validated finite element model. With D-0 as a typical specimen, the material model, unit type, interface simulation, and boundary conditions were identical to those in the validated finite element model. In total, 34 specimens were set in the parametric study. The effect of the eccentricity on the carrying capacity was examined by changing the thicknesses of the steel pipe and vertical steel plate. The axial carrying capacity (N_u) and bending momentum (M_u) in the middle section of the specimens were calculated to generate N-M curves with eccentricity. To determine the conservation by using LCFST-D columns, the N-M curves were obtained by normalizing the axial force and bending moment with the respective flexural and axial resistances (N_m and M_m) from the model, as shown in Fig. 21 (b) and Fig. 22 (b).

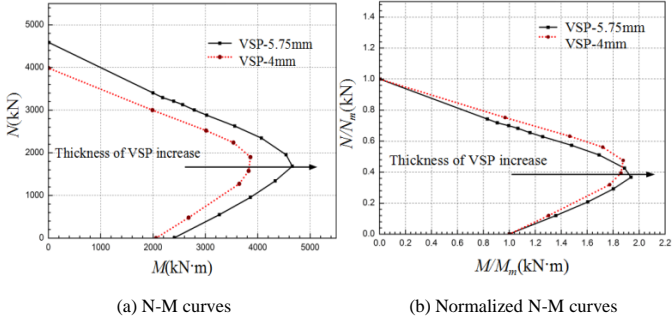


Fig. 21 Effects of the vertical steel plate thickness

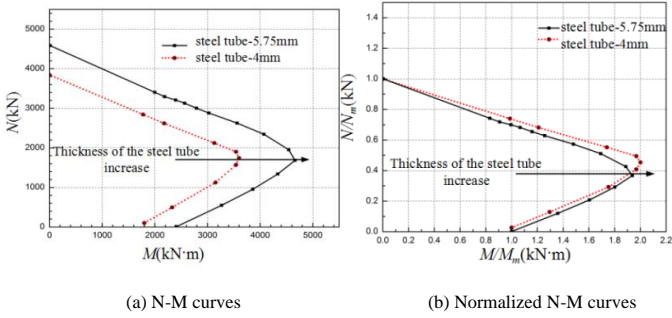


Fig. 22 Effects of the steel tube thickness

The effects of the thickness of the vertical steel plate on the LCFST-D columns are shown in Fig. 21. The carrying capacity decreased by 15.9% when the thickness of the vertical steel plate decreased from 5.75 mm to 4 mm because the narrow vertical steel plate decreased the moment of inertia of the components around the weak axis and increased the overall instability of the specimens. Additionally, the risks of partial buckling at the vertical steel plate increased, which decreased the bending moment and axial load. Thin vertical steel plates in the specimen design ultimately weakened the bending resistance.

The effects of the thickness of the steel pipe on the LCFST-D columns are shown in Fig. 22. As the thickness of the steel pipe decreased from 5.75 mm to 4 mm, the carrying capacity decreased by 19%. With the decrease in thickness of the steel pipe, partial buckling is likely to develop. The monocolumn is the first component in these columns that bears the load. The decrease in steel pipe thickness weakens the constraint of the inner concrete and makes monocolumns more likely to develop local buckling or instability. Therefore, the thickness of the steel pipe significantly affects the carrying capacity.

5. Discussion of the eccentric bearing capacity of the LCFST-D columns

5.1. Calculating the eccentric bearing capacity of the LCFST-D columns

This study proposes a formula to predict the eccentric carrying capacity of LCFST-D columns. The basic assumptions are as follows:

- The concrete and steel pipe undergo coordinated deformation.
- The strain of the cross-section maintains a linear distribution along the section height (i.e., the plane section assumption).
- The steels adopt the entire section plastic yield assumption, and the steel yield strength is f_y .
- Without considering the tensile contribution of the concrete, the force

analysis adopts the limit equilibrium theory.

e. The strength of concrete in the compression zone is f_{ck} of the standard value of the prism compressive strength.

Given the above assumptions, the failure phenomenon of this type of specimen is bending instability failure through eccentric compression. When the pressure point is on the Y'Y' axis, the bending deformation direction of the LCFST-D column rotates around the X'X' axis. As shown in Fig. 23, the calculation of the cross-section compression-bending capacity is divided into three cases:

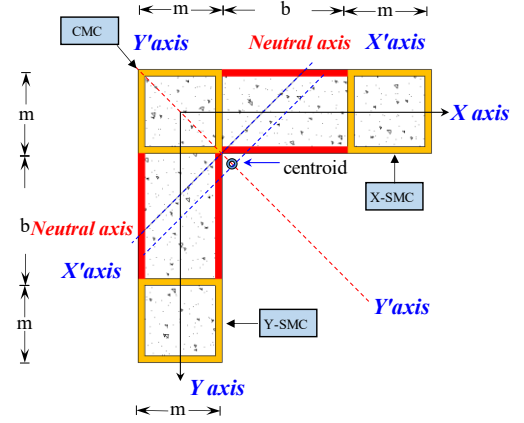


Fig. 23 Cross-sections of the LCFST-D column

$$N = \sum A_{st} f_y - \sum A_{sp} f_y - \sum A_{cp} f_c \quad (2)$$

$$M = \sum A_{st} f_y L_{st} - \sum A_{sp} f_y L_{sp} - A_{cp} f_c L_{cp} \quad (3)$$

(1) Calculation of ultimate bearing capacity in pure bending

Force balance:

$$\sum N = 0, \quad \sum A_{st} f_y - \sum A_{sp} f_y - \sum A_{cp} f_c = 0 \quad (4)$$

According to Eq. (4), The coordinates of the neutral axis can be solved.

$$M_{ux} = \sum A_{st} f_y L_{st} - \sum A_{sp} f_y L_{sp} - A_{cp} f_c L_{cp} \quad (5)$$

where A_{st} is the area of steel in the tensile zone; A_{sp} is the area of steel in the compression zone; A_{cp} is the area of concrete in the compression zone; L_{sp} is the distance between the point of action of the resultant force of the section area of steel in the compression zone and the centroid of the LCFST-D column; L_{st} is the distance between the point of action of the resultant force of the section area of steel in the tension area and the centroid of the LCFST-D column; and L_{cp} is the distance between the point of action of the resultant force of the section area of concrete in the compression zone and the centroid of the LCFST-D column.

(2) Calculation of the stable bearing capacity of the LCFST-D columns

The L-shaped column is a uniaxially symmetrical member, and its unidirectional bending failure may cause two types of failure: torsional failure and bending failure. In this experiment, the bias point of the LCFST-D column is on the Y'Y' axis, and its failure phenomenon is bending failure. The failure type of the specimen is bending instability failure around the weak axis (X'X' axis). This paper proposed formulas to calculate the stable carrying capacity (Eqs. (6)-(10)) with bending buckling instability failure.

$$\frac{N}{\Phi_x N_u} + (1 - \alpha_c) \frac{\beta M_{x'}}{(1 - 0.8 \frac{N}{N_{Ex}}) M_{ux}} = 1 \quad (6)$$

$$N'_{Ex} = \frac{N_{Ex}}{1.1} \quad (7)$$

$$N_{Ex} = N_u \frac{\pi^2 E_c}{\lambda_x^2 f} \quad (8)$$

$$\alpha_c = \frac{f_c A_c}{f A_s + f_c A_c} \quad (9)$$

$$N_u = A_s f + A_c f_c \quad (10)$$

where N is the design value of the axial compressive force in the range of the calculated component section; M is the design value of the bending moment; α_c is the concrete work bearing coefficient; M_{ux} is the design value of the bending capacity of the net section when only the bending moment M_x acts, which is calculated using formula (5); N_{Ex} is the Euler critical force; β is the equivalent bending moment coefficient, which is generally 1; and φ_x is the stability coefficient around the X'X' axis, which is calculated by a formula in the literature [39–40].

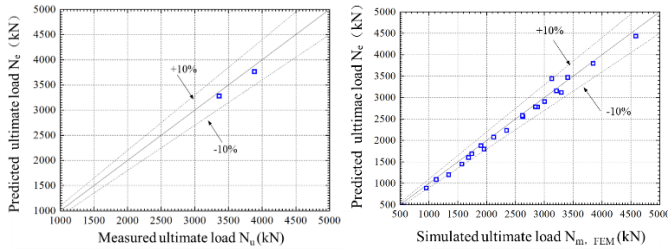


Fig. 24 Predicted N_e versus test results Fig. 25 Predicted N_e versus simulation results

Fig. 24 shows a comparison between the calculated and measured ultimate loads, where N_e is the peak load calculated by the proposed formula in this article, and N_u is the measured peak load of this test. The average value of N_e/N_u was 0.973, the average error was less than 5%, and the standard deviation was 0.00326. The calculation values were lower than but consistent with the test values. Therefore, the calculated value obtained using this calculation method was more conservative than the actual bearing capacity. Fig. 25 shows a comparison of the predicted N_e and $N_{m,FEM}$, where $N_{m,FEM}$ was obtained from the finite element simulations. The average value of $N_e/N_{m,FEM}$ is 0.947, the error was less than 10%, and the standard deviation was 0.0492. The analysis found that the value calculated by this formula has small errors with $N_{m,FEM}$ and N_u , which indicates that the calculation method can accurately predict the eccentric carrying capacity.

References

- [1] Han, L.H., An, Y.F., "Performance of concrete-encased CFST stub columns under axial compression", *Journal of Constructional Steel Research*, 93, 62–76, 2014.
- [2] Chen Z.H., Qin Y., Wang X.D., "Development of connections to concrete-filled rectangular tubular columns", *Advanced Steel Construction*, 11(4), 408–426, 2015.
- [3] M.Longshithung Patton, Konjengbam Darunkumar Singh., "Finite Element Modelling of Concrete-filled Lean Duplex Stainless Steel Tubular Stub Columns", *International Journal of Steel Structures*, 14(3), 619–632, 2014.
- [4] Li, G.C., Di, C.Y., Tian, L., et al. "Nonlinear finite element analysis on long columns of high-strength concrete-filled square steel tube with inner CFRP circular tube under axial load", *Advanced Steel Construction*, 9(2), 124–138, 2013.
- [5] Liu, X.G., Liu, J.P., Yang, Y.L., et al. Resistance of special-shaped concrete-filled steel tube columns under compression and bending[J]. *Journal of Constructional Steel Research*, 169, 106038, 2020.
- [6] Bai, Y.T., Lin, X.C. and Ben M., "Numerical Modeling on Post-Local Buckling Behavior of Circular and Square Concrete-Filled Steel Tubular Beam Columns", *International Journal of Steel Structures*, 16(2), 531–546, 2016.
- [7] Yu, F., He, S., Niu, D. "Study on unified bearing capacity of rectangular concrete-filled steel tubular column subjected to axial compression", *Advanced Steel Construction*, 8(1), 95–111, 2012.
- [8] Ren, Q.X., Han, L.H., Hou, Ch., and Hua Y.X., "Experimental behaviour of tapered CFST columns under combined compression and bending", *Journal of Constructional Steel Research*, 128, 39–52, 2017.
- [9] Du, Y.S., Chen, Z.H., J.Y. Richard Liew, and Xiong, M.X., "Rectangular concrete-filled steel tubular beam-columns using high-strength steel: Experiments and design", *Journal of Constructional Steel Research*, 131, 1–18, 2017.
- [10] Guler, S., Çopur, A., Aydoğan, M., "A Comparative study on square and circular high strength concrete-filled steel tube columns", *Advanced Steel Construction*, 10(2), 234–247, 2014.
- [11] Han, L.H., "Concrete-filled steel tubular structures: theory and practice", Beijing: Science Press, 2007. (in Chinese)
- [12] Masaru, S., Fumihito, T., Toshiyuki, I., Atsushi, H., and Hirotaka, K., "Experimental Study on Ultimate Strength of Concrete Filled Double Tubular Steel with Shear Connector", *International Journal of Steel Structures*, 13(3), 49–54, 2013.
- [13] Hu, J.W., Park, J., Leon, R.T., "Advanced analysis and performance based evaluation of concrete filled tube (CFT) columns", *Advanced Steel Construction*, 6 (4), 1019–1033, 2010.
- [14] Qin, Y., Chen, Z.H., and Han, N., "Research on Design of Through-Diaphragm Connections between CFRT Columns and HSS Beams", *International Journal of Steel Structures*, 9(14), 589–600, 2014.
- [15] Guo, Y., and Yao, X., "Seismic performance and design of reduced steel beam section with concrete filled square tubular column", *Advanced Steel Construction*, 9(3), 173–189, 2013.
- [16] Tao Z, Wang Z-B, Yu Q. "Finite element modelling of concrete-filled steel stub columns

6. Summary and conclusion

According to the eccentric compression experiments and analysis of these LCFST-D columns, we draw the following conclusions:

1. The LCFST-D columns had high ductility and bearing capacity under eccentric loading. The bearing capacity gradually decreased with increasing eccentricity, whereas the ductility slightly increased. The plastic deformation capacity of the section was high, and the three monocolumns shared loads well.

2. With identical eccentricity and other conditions, these LCFST-D columns had a notably higher carrying capacity than the LCFST columns. The carrying capacity of D-0 was 21.3% higher than that of E-0, the carrying capacity of D-40 was 60% higher than that of E-40, and the carrying capacity of D-80 was 65.5% higher than that of E-80. Compared to the single steel plate, the concrete in the double vertical steel plates effectively enhanced the monocolumn coordination and internal force transmission, prevented the primitive buckling of the vertical steel plates and better utilized the material properties.

3. Eccentric compression was simulated by ANSYS. The emulation results were consistent with the experimental results. Under eccentric loads, the three monocolumns first carried the load. The stress at the vertical steel plate gradually increased with increasing load, and the middle total cross-section yielded at the peak load, which indicates that the plasticity of the materials could be completely utilized. The N-M curves of the LCFST-D columns were obtained through a parametric analysis of the thickness of the steel pipe and vertical steel plate based on the validated finite element model. The thickness of the steel pipe was the major influencing factor. The flexural capacity could be increased during structural design by increasing the thickness of steel pipes.

4. When the eccentricity direction was the axis of symmetry of the LCFST-D column, its failure type was bending instability failure around the weak axis (X'X' axis). Thus, this paper proposed a simplified calculation formula to predict the compression and bending carrying capacity. The calculation results were consistent with the test values, and the error was less than 10%, which can provide a reference for engineering design.

Acknowledgements

This work was sponsored by the National Natural Science Foundation of China (52008270), the Youth Program of the Natural Science Foundation of Hebei Province, China (grant Nos. E2019210094 and E2020210003), and the Youth Project of the Science and Technology Research Foundation of Hebei Colleges and Universities, China (grant Nos. QN2018246 and QN2020409).

- under axial compression", *Journal of Constructional Steel Research*, 89, 121–31, 2013.
- [17] Xiong Q.Q., Chen Z.H., Kang J.F., Zhou T., Zhang W., "Experimental and finite element study on seismic performance of the LCFSTD columns", *Journal of Constructional Steel Research*, 137, 119–134, 2017.
- [18] Xiong Q.Q., Chen Z.H., Zhang W., Zhou T., Kang J.F., "Compressive behaviour and design of L-shaped columns fabricated using concrete-filled steel tubes", *Engineering Structures*, 152, 758–770, 2017.
- [19] Tu, Y.Q., Shen, Y.F., and Li, P., "Behaviour of multi-cell composite T-shaped concrete-filled steel tubular columns under axial compression", *Thin-Walled Structures*, 85, 57–70, 2014.
- [20] Rong, B., Feng, C.X., Zhang, R.Y., You, G.C., and Liu R., "Compression-bending Performance of L-shaped Column Composed of Concrete Filled Square Steel Tubes under Eccentric Compression", *International Journal of Steel Structures*, 17, 1, 325–337, 2017.
- [21] Tu, Y.Q., Shen, Y.F., Zeng, Y.G., and Ma, L.Y., "Hysteretic behavior of multi-cell T-shaped concrete-filled steel tubular columns", *Thin-Walled Structures*, 85, 106–116, 2014.
- [22] Wang, Y.Y., Yang, Y.L., and Zhang, S.M., "Static behaviors of reinforcement-stiffened square concrete-filled steel tubular columns", *Thin-Walled Structures*, 58, 18–31, 2012.
- [23] Yang, Y.L., Zhang, H., and Zhang, S.M., "Compressive Behavior of T-shaped Concrete Filled Steel Tubular Columns", *International Journal of Steel Structure*, 9, 10, 419–430, 2010.
- [24] Yang, Y.L., Wang, Y.Y., and Fu, F., "Effect of reinforcement stiffeners on square concrete-filled steel tubular columns subjected to axial compressive load", *Thin-Walled Structures*, 82, 132–144, 2014.
- [25] Yang, Y.L., Wang, Y.Y., Fu, F., and Liu, J.C., "Static behavior of T-shaped concrete-filled steel tubular columns subjected to concentric and eccentric compressive loads", *Thin-Walled Structures*, 95, 374–388, 2015.
- [26] Zuo, Z.L., Cai, J. C., Chen, Q. J., "Eccentric load behavior of L-shaped CFT steel tube columns with binding bars", *Journal of Constructional Steel Research*, 72, 105–118, 2012.
- [27] Cai, J. and He, Z.Q., "Axial load behavior of square CFT stub column with binding bars", *Journal of Constructional Steel Research*, 62, 5, 472–83, 2006.
- [28] Lin, Z.Y., Shen, Z.Y., Luo, J.H., and Zhang, J.C., "Study on behavior of L-shaped concrete-filled steel tube stubs subjected to axial compression", *Progress Steel Build Structures*, 11, 6, 14–9, 2009. (in Chinese)
- [29] Chen, Z.H. and Rong, B., "Axial compression stability of a crisscross section column composed of concrete-filled square steel tubes", *Journal of Mechanics of Materials and Structures*, 4 (10), 1787–1799, 2009.
- [30] Chen, Z.H., Li, Z.Y., Rong, B., and Liu, X.L., "Experiment of axial compression bearing capacity for crisscross section special-shaped column composed of concrete-filled square steel tubes", *Journal of Tianjin University*, 39(11), 1275–128, 2006. (in Chinese)
- [31] Rong, B., Chen, Z.H., Apostolos, F., Yang, N., "Axial compression behavior and analytical method of L-shaped column composed of concrete-filled square steel tubes", *Transactions of Tianjin University*, 18(3), 180–187, 2012.
- [32] Zhou, T., Xu, M.Y., Wang, X.D., Chen, Z.H., and Qin, Y., "Experimental Study and Parameter Analysis of L-shaped Composite Column under Axial Loading", *International Journal of*

- Steel Structures, 15, 4, 797-807, 2015.
- [33] Xu, M.Y., Zhou, T., Chen, Z.H., Li, Y.B., and Luke Bisby., "Experimental study of slender LCFST columns connected by steel linking plates", *Journal of Constructional Steel Research*, 127, 231–241, 2016.
- [34] GB50010-2010. "Code for design of concrete structures (2010)", China Association for Engineering Construction standardization. (in Chinese)
- [35] Xiong Q.Q., Zhang W., Chen Z.H., Du Y.S., Zhou T., "Experimental Study of the Shear Capacity of Steel Beam-to-L-CFST Column Connections", *International Journal of Steel Structures*, 19(3), 704–718. 2019.
- [36] Fukumoto T, Morita K., "Elasto plastic behavior of steel beam to square concrete filled steel tube (CFT) column connections", *Proceedings of the 6th ASCCS Conference Vol. 1: Composite and Hybrid Structures*. Los Angeles, USA, 565-572, 2000.
- [37] Ellobody, B. Young, Nonlinear analysis of concrete-filled steel SHS and RHS columns, *Thin Walled Structure*. 44, 919-930, 2006.
- [38] Zhao Z.W., Zhang H.W. Xian L.N., Liu H.Q., "Tensile strength of Q345 steel with random pitting corrosion based on numerical analysis", *Thin-walled structures*, 2020, 148, 106579.
- [39] GB50017-2003. "Code for design of steel structures", China Ministry of Construction, 2003. (in Chinese)
- [40] Zhang W., Chen Z.H., Xiong Q.Q., "Performance of L-shaped columns comprising concrete-filled steel tubes under axial compression", *Journal of Constructional Steel Research*, 145, 573–590, 2018.